Acta Materialia 124 (2017) 100–108

Contents lists available at ScienceDirect

Acta Materialia

journal homepage: www.elsevier.com/locate/actamat

Full length article

Uncertainty quantification of microstructural properties due to variability in measured pole figures

Pınar Acar, Veera Sundararaghavan*

Aerospace Engineering, University of Michigan, Ann Arbor, 48109, MI, USA

ARTICLE INFO

Article history:
Received 20 May 2016
Received in revised form
26 October 2016
Accepted 28 October 2016
Available online 11 November 2016

Keywords:
Uncertainty quantification
Probability
Microstructure

ABSTRACT

Experimental pole figures are an important input for microstructure homogenization models. In this paper, we derive an exact analytical formulation to quantify the uncertainties in homogenized properties due to uncertainty in the experimentally measured pole figures. The pole figures are acquired from a set of Ti-7Al alloy samples. These samples were obtained from the same process: by compressing a beta forged ingot at room temperature followed by annealing. The samples were taken from different regions of the original ingot, and this created variability in the resulting pole figures. The joint multivariate probability distributions of the computed orientation distribution function (ODF) is then found using the method of characteristic functions based on a Gaussian model of the pole figures. Engineering properties such as elastic modulus can be obtained by volume averaging over the ODF. We also show that uncertainty in elastic properties can be analytically obtained using direct transformation of random variables in the homogenization approach.

1. Introduction

Integrated Computational Materials Engineering (ICME) (Allison et al. [1]) is an emerging paradigm for materials design that emphasizes integration of material models at multiple length scales with engineering analysis of products and processes. Critical inputs of these material models come from experiments, for example, initial orientation distribution function of the polycrystalline structure is a key input for multiscale crystal plasticity models. However, microstructures are inherently stochastic in nature. In other words, specimens made from the same manufacturing process have variations in microstructure both point-to-point in one specimen and across all specimens. One of the pillars of ICME is uncertainty quantification (UQ) and involves development of mathematical tools to quantify the effect of stochasticity of microstructure on the predicted engineering properties.

Current state of the art involves the use of expensive numerical simulations such as Monte Carlo simulations (MCS), collocation and spectral decomposition methods to quantify the uncertainties. Creuziger et al. [2] examined the uncertainties in the orientation distribution function (ODF) values of a microstructure due to the variations in the pole figure (PF) values by using Monte Carlo Simulation (MCS). Juan et al. [3] used MCS to study effects of sampling strategy on the determination of various characteristic microstructure parameters such as grain size distribution and grain topology distribution. Hiriyur et al. [4] studied an extended finite element method (XFEM) coupled with an MCS approach to quantify the uncertainties in the homogenized effective elastic properties of multiphase materials. The uncertain parameters were assumed to be aspect ratios, spatial distribution and orientation. They used a strain energy approach to analyze the uncertainties of in-plane Young's modulus and Poisson's ratio. Kouchmeshky and Zabaras [5] presented propagation of initial texture and deformation process uncertainties on the final product properties. They used a data-driven approach to identify the joint probability distributions of random variables with Maximum Entropy Method, and modeled the stochastic problem using a stochastic collocation approach. Madrid et al. [6] examined the variability and sensitivity of in-plane Young's modulus of thin nickel polycrystalline films due to uncertainties in microstructure geometry, crystallographic texture, and numerical values of single crystal elastic constants by using a numerical spectral technique. Niezgoda et al. [7] computed the variances of the microstructure properties by defining a stochastic process to represent the microstructure. They marked the sensitive regions in the convex hull generated with Principal Component Analysis (PCA), and calculated the probability

* Corresponding author.
E-mail address: veeras@umich.edu (V. Sundararaghavan).

http://dx.doi.org/10.1016/j.actamat.2016.10.070
1359-6454/

distributions of stiffness and yield stress in case of low, medium and high variances.

These computational methods presented in literature involve using a numerical algorithm for uncertainty quantification and propagation. They represent the joint probability distributions of uncertain variables either using interpolation functions or sampling for random points. These techniques are not computationally efficient as the problem complexity or the number of variables increases since the number of interpolation terms or sampling points will also increase. This is especially true for orientation distribution functions that are discretized using finite element nodes or spectral basis and contain large number of free parameters whose joint distribution needs to be sampled. Another drawback is the difficulty of satisfying design constraints (such as volume fraction normalization) when using numerical approaches. Finally, these methods do not take advantage of the linear transformations involved in the conversion of pole figures to ODFs [8] that allow analytical representations of uncertainty under certain cases. All these disadvantages imply the necessity of developing analytical solutions as a first step in UQ.

In this work, we develop a set of analytical formulae to quantify uncertainty in the ODF due to variability in the measured pole figures. This uncertainty is 'aleatoric' [9] and arises from variations in texture across specimens subject to the same process. The measurements were taken across different beta forged Ti-Al samples that were subject to the same compression and annealing process. The measurements were also taken from different regions of these samples. The probability distributions of the PFs were computed from these scans and were found to be roughly Gaussian in nature. Then, the propagation of uncertainties on the ODFs are computed using an analytical formulation. Note that pole figure inversion is non-unique and several numerical methods have been developed for this purpose dating back to Bunge (1969) [10]. These different methods lead to a band of solutions for the true ODF. In the UQ community, the uncertainty that arises from lack of an exact solution is classified as 'epistemic' uncertainty [9], and such an uncertainty is not considered in this work. In this context, Randle and Engler [11] classified various inversion methods to categories of 'harmonic' or 'direct' methods and compared the methods against each other. While all methods were found to yield reproducible results, it was suggested to stay with a given method during a series of experiments. In this work, we stay within the least squares minimization method of Barton et al. [8] to compute the ODF. The secondary uncertainty that comes from the X-ray instrument itself is also not considered. Once the uncertainty in the ODF is quantified, we present an approach to identify the probability distributions of the material properties that are derived from the ODF such as Young's modulus and shear modulus using the random variable transformation method. The organization of this paper is as follows. Section 2 discusses the problem statement. In Section 3, the mathematical methods are described. Results and conclusions are addressed in Sections 4 and 5 respectively.

2. Mathematical background

The complete orientation space of a polycrystal can be reduced to a smaller subset, called the fundamental region, as a consequence of crystal symmetries. Within the fundamental region, each crystal orientation is represented uniquely by a coordinate $\boldsymbol{r}$, the parametrization for the rotation (eg. Euler angles, Rodrigues vector etc.). The ODF, represented by $\mathcal{A}(\boldsymbol{r})$, describes the volume density of crystals of orientation $\boldsymbol{r}$. The ODF representation in the Rodrigues fundamental region for Titanium (hcp) is shown in Fig. 1 and the locations of the k independent nodes are shown. The volume density of any other node in the fundamental region can be

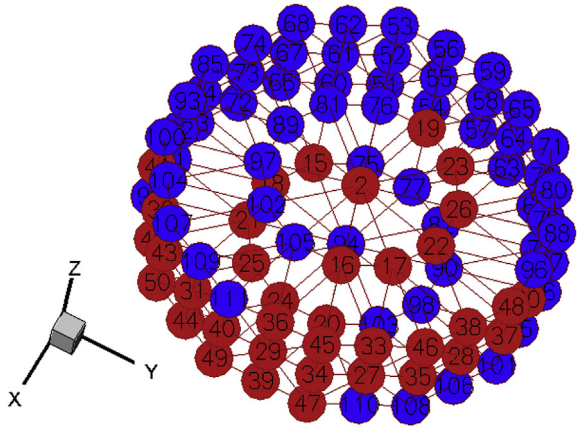

Fig. 1. ODF representation in the Rodrigues fundamental region for hexagonal crystal symmetry showing the location of the k = 50 independent nodes of the ODF in red color. (For interpretation of the references to colour in this figure legend, the reader is referred to the web version of this article.)

obtained from these independent nodes through symmetry. The ODF also satisfies a normalization constraint, $\int \boldsymbol{A} dv = 1$, with the integral computed over the fundamental region. The normalization constraint can be written as a linear equation of the form $\sum_{i=1}^{k} q_i A_i = 1$ (see Appendix A), with A_i denoting the ODF value at node i.

The experimentally obtained pole figure for a particular diffraction plane unit normal $\boldsymbol{h}$ contains the pole density function $P(\boldsymbol{h},\boldsymbol{y_i})$ measured at locations $\boldsymbol{y_1},\boldsymbol{y_2}, \ldots,\boldsymbol{y_q}$ on a unit sphere. The value of $P(\boldsymbol{h},\boldsymbol{y_i})$ at location $\boldsymbol{y_i}$ can be computed from the ODF ($\boldsymbol{A}$) using a single linear equation based on the algorithm of Barton et al. [8]:

$$P(h, y_i) = \sum_{j=1}^{k} M_{ij} A_j \tag{1}$$

where M_{ij} are the values from a known system matrix $\boldsymbol{M}$. One such equation can be written for each of the m points in a pole figure. This set of equations can be combined with a similar set of equations for n other pole figures with different diffraction normals $\boldsymbol{h}$. This leads to a global system of equations $\boldsymbol{P} = \boldsymbol{MA}$. Here, $\boldsymbol{P}$ is a column vector of size $m \times n$, $\boldsymbol{M}$ is a matrix of size $(mn) \times (k)$ and the ODF $\boldsymbol{A}$ is a column vector of size k containing the volume densities of k independent nodes. In order to account for the normalization constraint $\sum_{i=1}^{k} q_i A_i = 1$, the overall system $\boldsymbol{P} = \boldsymbol{MA}$ is adjusted such that $M_{ij} = M_{ij} - \frac{M_{ik} q_j}{q_k}$ for $j = 1, \ldots, k-1$ and $P_i = P_i - \frac{M_{ik}}{q_k}$.

The system of equations is over–determined (ie. more pole figure data as compared to the unknown ODF values) and direct inversion is not possible. Instead following Barton et al. [8], the ODF is retrieved from the experimental pole figures using least squares minimization as follows:

$$\boldsymbol{A} = \boldsymbol{CP} \tag{2}$$

where the coefficient matrix, $\boldsymbol{C} = (\boldsymbol{M^T M})^{-1} \boldsymbol{M^T}$ is the pseudo–inverse.

If the orientation-dependent property for single crystals, $\boldsymbol{\chi}(\boldsymbol{r})$, are known, any polycrystal property can be expressed as an expected value, or average, over the ODF as follows:

$$< \boldsymbol{\chi} > = \int \boldsymbol{\chi}(\boldsymbol{r}) \boldsymbol{A}(\boldsymbol{r}) dv \,, \tag{3}$$

Other properties may be derived from $<\chi>$. For example, the elastic modulus can be written as $E = \frac{1}{<S_{11}>}$ where $<S_{11}>$ is a component of the compliance matrix ($\boldsymbol{S}$) computed from the lower bound relation $<\boldsymbol{S}> = \int_R \boldsymbol{S}(\boldsymbol{r})\boldsymbol{A}(\boldsymbol{r})dv$.

2.1. Problem statement

Polycrystalline microstructures are inherently stochastic in nature. Specimens made from the same manufacturing process have variations in microstructure across point-to-point within one specimen as well as across all specimens. This variability can be quantified by using diffraction experiments to measure pole figures at different locations (leading to known uncertainty in the vector $\boldsymbol{P}$ in Eq. (2)). Given this measurement uncertainty in the pole figures, the primary goals of this article is to:

(1) Develop analytical expressions for the probability distribution function of the ODF values.
(2) Compute the uncertainty in properties derived from the homogenization equation (3) given the uncertainty in the ODF.

The probabilistic methods employed are explained next.

3. Methods

In this work, three pole figures (h = <001>, <010> and <101>, $n = 3$) for a Titanium alloy were considered. The variability in the pole density function $P(\boldsymbol{h},\boldsymbol{y_i})$ at each point $\boldsymbol{y_i}$ for these three pole figures were computed from 100 different samples drawn from the specimen. The histograms of these variations were plotted and we found the variability in $P(\boldsymbol{h},\boldsymbol{y_i})$ to have Gaussian features as shown in Fig. 2.

Since the experimental samples show that the variations in the PFs are consistent with Gaussian distribution, the solution approach depends on two steps. The first being to prove that the variations in the ODFs are also consistent with Gaussian distribution. The second step is to compute the mean value and standard deviation of the joint multivariate distributions for the ODFs. Once the distribution type and statistical quantities are determined the variation in the output variables can be identified. Considering the linear relation in Eq. (2), the derivation of the joint multivariate probability distribution is discussed below for a general case with $\boldsymbol{d}$ Gaussian random variables using Method of Characteristic Functions [12].

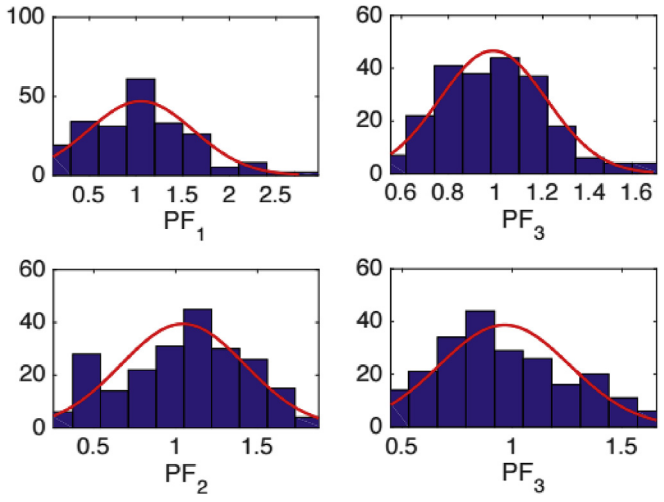

Fig. 2. Probability histograms of a few representative pole density values ($P(\boldsymbol{h},\boldsymbol{y_i})$). The labels indicate the PF1, PF2 and PF3 indicate the pole figures h = <001>, <010> and <101> respectively from which these densities are obtained.

3.1. Method of characteristic functions

Assume a d-dimensional multivariate normal distribution: $\boldsymbol{X} \sim \boldsymbol{N_d}(\boldsymbol{\mu}, \boldsymbol{\Sigma})$, where vector of mean values $\boldsymbol{\mu}=(\mu_1, \ldots,\mu_d)^T = E[\boldsymbol{X}]$ and covariance matrix $\Sigma_{jk} = cov(X_j, X_k) = E[(X_j - \mu_j)(X_k - \mu_k)]$, $j,k = 1, \ldots,d$ are known. The characteristic function for the Gaussian distributed variable, $\boldsymbol{X}$, is given by:

$$\psi_X(t) = E\left[exp\left(i\boldsymbol{t^T X}\right)\right] = exp\left(i\boldsymbol{t^T \mu_X} - \frac{1}{2}\boldsymbol{t^T \Sigma_X t}\right)$$
$$= exp\left(i\sum_{j=1}^{d} t_j\mu_j - \frac{1}{2}\sum_{j=1}^{d}\sum_{k=1}^{d} t_j t_k \Sigma_{jk}\right) \quad (4)$$

For a one-dimensional Gaussian variable, $Y \sim N_1(\mu_y, \sigma_y^2)$:

$$\psi_Y(t) = exp\left(it^T\mu_y - \frac{1}{2}t^2\sigma_y^2\right) \quad (5)$$

Now we define a new random variable,

$$Z = \boldsymbol{a^T X} = \sum_{j=1}^{d} a_j X_j \quad (6)$$

where $\boldsymbol{a}$ is a constant column vector. The characteristic function for Z is given by:

$$\psi_Z(t) = E[exp(itZ)] = E\left[exp\left(it\boldsymbol{a^T X}\right)\right] = \psi_X(t\boldsymbol{a}) \quad (7)$$

$$\psi_Z(t) = exp\left(it\sum_{j=1}^{d} a_j\mu_j - \frac{1}{2}t^2\sum_{j=1}^{d}\sum_{k=1}^{d} a_j a_k \Sigma_{jk}\right) \quad (8)$$

The comparison of this new characteristic function, $\psi_Z(t)$, with the characteristic function for the one-dimensional variable, $\psi_Y(t)$, shows that they are almost equivalent, except μ_y is replaced by $\mu_z = \sum_{j=1}^{d} a_j\mu_j = \boldsymbol{a^T \mu_X}$, and σ_y^2 is replaced by $\sigma_z^2 = \sum_{j=1}^{d}\sum_{k=1}^{d} a_j a_k \Sigma_{jk} = \boldsymbol{a^T \Sigma_X a}$. Since the characteristic function of Z is equivalent to the characteristic function of Y, the distributions must also be equal. Therefore, Z is also Gaussian distributed. The above derivation can be generalized to a matrix–vector product, $\boldsymbol{Z} = \boldsymbol{AX}$. The characteristic function for vector $\boldsymbol{Z}$ is given by:

$$\psi_Z(t) = E\left[exp\left(it^T\boldsymbol{Z}\right)\right] = E\left[exp\left(it^T\boldsymbol{AX}\right)\right] = \psi_X\left(\boldsymbol{A}^T t\right) \quad (9)$$

$$\psi_Z(t) = exp\left(i\boldsymbol{t^T A\mu_X} - \frac{1}{2}\boldsymbol{t^T A\Sigma_X A^T t}\right) \quad (10)$$

Here, the mean and covariance of vector $\boldsymbol{Z}$ is given by:

$$\boldsymbol{\mu_Z} = \boldsymbol{A\mu_X} \quad (11)$$

$$\boldsymbol{\Sigma_Z} = \boldsymbol{A\Sigma_X A^T} \quad (12)$$

3.2. Computation of the ODF uncertainty

From Eq. (2), the ODF is retrieved from the equation $\boldsymbol{A} = \boldsymbol{CP}$.

From the known mean vector ($\boldsymbol{\mu_P}$) and covariance matrix ($\boldsymbol{\Sigma_P}$) of the pole density vector $\boldsymbol{P}$ obtained from experiments, the mean and covariance matrix of the ODF $\boldsymbol{A}$ can be computed using Eq. (11) and Eq. (12) as $\boldsymbol{\mu_A} = \boldsymbol{C\mu_P}$ and $\boldsymbol{\Sigma_A} = \boldsymbol{C\Sigma_P C^T}$. These expressions give the mean values and covariance matrix of the first $k-1$ independent ODF values. The PDF of the kth ODF value is then computed using the normalization constraint. Knowing the volume density of the first $k-1$ nodes, the volume density of the kth node can be found as:

$$A_k = \sum_{i=1}^{k-1} c_i A_i + \frac{1}{q_k}, \text{ where } c_i = -\frac{q_i}{q_k} \tag{13}$$

This is similar to the linear equation (6) with an added constant, and mean and variances can be obtained as $\mu_k = \boldsymbol{c^T \mu_A} + \frac{1}{q_k}$ and variance of $\sigma_k^2 = \boldsymbol{c^T \Sigma_A c}$.

Remark: The full covariance matrix $\boldsymbol{\Sigma_A^*}$ of k independent nodes of the ODF can also be computed as a postprocessing step, but is not required for property analysis. The covariance matrix of the first $k-1$ independent ODF values $\boldsymbol{\Sigma_A}$ is a $(k-1) \times (k-1)$ square matrix. The full covariance matrix is a $k \times k$ square matrix given by:

$$\boldsymbol{\Sigma_A^*} = \begin{bmatrix} \boldsymbol{\Sigma_A} & \boldsymbol{S} \\ \boldsymbol{S^T} & \sigma_k^2 \end{bmatrix} \tag{14}$$

where, $\boldsymbol{S}$ is a column vector whose values are given by

$$S_i = -\frac{1}{q_k} \sum_{j=1}^{k-1} q_j (\Sigma_A)_{ij} \tag{15}$$

3.3. Computation of uncertainty in linear properties

The next step is to identify the probability distributions of the material properties. Elements of the compliance matrix can be computed using an averaged linear relation in terms of the ODFs $<S_{11}> = \int S_{11} A dV$ which can be written in the form $S_{11} = \boldsymbol{p^T A} + r$ (see appendix). Since the ODFs are already identified as Gaussian distributed, these linear relations imply that the probability distributions of compliance components such as $<S_{11}>$ and $<S_{66}>$ are also Gaussian, and their mean values and standard deviations can be computed as $\mu_{S_{11}} = \boldsymbol{p^T \mu_A} + r$, and $\sigma_{S_{11}}^2 = \boldsymbol{p^T \Sigma_A p}$ using Eq. (8).

3.4. Uncertainties in the material properties for nonlinear properties

When the probability distribution of a property is not linear in the ODF, the PDF can still be computed using Transformation of Random Variables. Given the input parameter, x, and the output parameter, y, we assume that the relation between x and y can be identified using $y = h(x)$, and can be inverted as $x = u(y)$. This method computes a Jacobian value, J, based on this explicit relation (where $J = du/dy$), and finds the PDF of the output variable as a product of input PDF and the Jacobian. Eq. (16) shows the computation of output PDF:

$$f_y(y) = f_x[u(y)] \times \left| J \right| \tag{16}$$

where f_x and f_y are the PDFs of input and output variables respectively. Since the input PDF, f_x, and inverted function, $u(y)$ are already known, the output PDF, f_y, can be computed using this method. Then, the expected value, $E[y]$, and variance, $\mathrm{Var}(y)$, of the output parameter can be calculated using Eqs. (17) and (18) respectively [13].

$$E[y] = \int_{y_{min}}^{y_{max}} y\, f_y(y) dy \tag{17}$$

$$Var(y) = E\left[(y - E[y])^2\right] \tag{18}$$

where $y_{\min}$ and $y_{\max}$ are the minimum and maximum values of the output variable, y, can take. These values can be computed using the relation $y = h(x)$ for the minimum and maximum values of the input variable, $x_{\min}$ and $x_{\max}$ respectively. The approach is demonstrated in the next section for computing the non–Gaussian PDF of the homogenized elastic modulus $E_1 = 1/S_{11}$ and shear modulus $G_{12} = 1/S_{66}$.

4. Results and discussion

This section discusses quantification of uncertainties in the ODF due to the texture variations across experimental samples. The material studied is Ti-7wt%Al which is an alpha titanium alloy with a beta transus temperature of 1050 °C. The alloy was forged from a 7.5 inch round ingot to a 4 inch square ingot at 1142 °C and air cooled. Three different cylindrical samples 6 mm in diameter and 9 mm in height were machined from the forged ingot. The samples were then subject to the same process: compression to a 20% height reduction at a strain rate of 0.03 mm/min ($5 \times 10^{-5}\ s^{-1}$) at room temperature followed by annealing in a tube furnace at 800 °C for 72 h followed by a water quench. The samples were sectioned perpendicular to the compression axis, mounted in epoxy and polished to a final step of colloidal silica. Scans were also taken from different regions of the processed samples to capture the texture uncertainty within each specimen. A total of hundred pole figures ($\boldsymbol{h}$ = <001>, <100> and <101>) were obtained from these scans. Microstructural variations arise due to stress and temperature gradient variabilities during processing of the raw material. Therefore, samples taken from different regions of an ingot that are subsequently annealed may have varying degrees of internal stresses which affects the resulting degree of recrystallization and texture. Uncertainties can also arise from heat loss through the mechanical press anvils during forging and variations in compression height between each forging step. Another source for variability is due to the temperature gradient that exists within the tube furnace. Therefore, slight differences in furnace location can create variations in annealing temperature from specimen to specimen. These variations exist across different specimens as well as point-to-point within a single specimen. Such variabilities are the primary sources of error in computational models that use a single microstructure representation (rather than a statistical distribution) to compute material properties.

Representative samples for the PFs obtained are illustrated in Fig. 3, and indicate a weakly basal texture. We consider $m = 221$ pole densities for each pole figure. Since three pole figures were sampled, a total of 663 pole density values in total were used in the UQ model. The HCP fundamental region discretized with 50 independent nodes as shown in Fig. 1 is used to model the ODF. To show the statistical features, the mean values and coefficient of variations (ratio of standard deviation to the mean value) of the PFs are depicted in Fig. 4 and Fig. 5 respectively.

Using Method of Characteristic Functions, the mean values and standard deviations of the ODFs are identified. We first solved for the probability distributions of the 49 ODF values, and then computed the probability distribution of the last ODF, ODF_{50}, by using the normalization constraint. The histograms for some of the

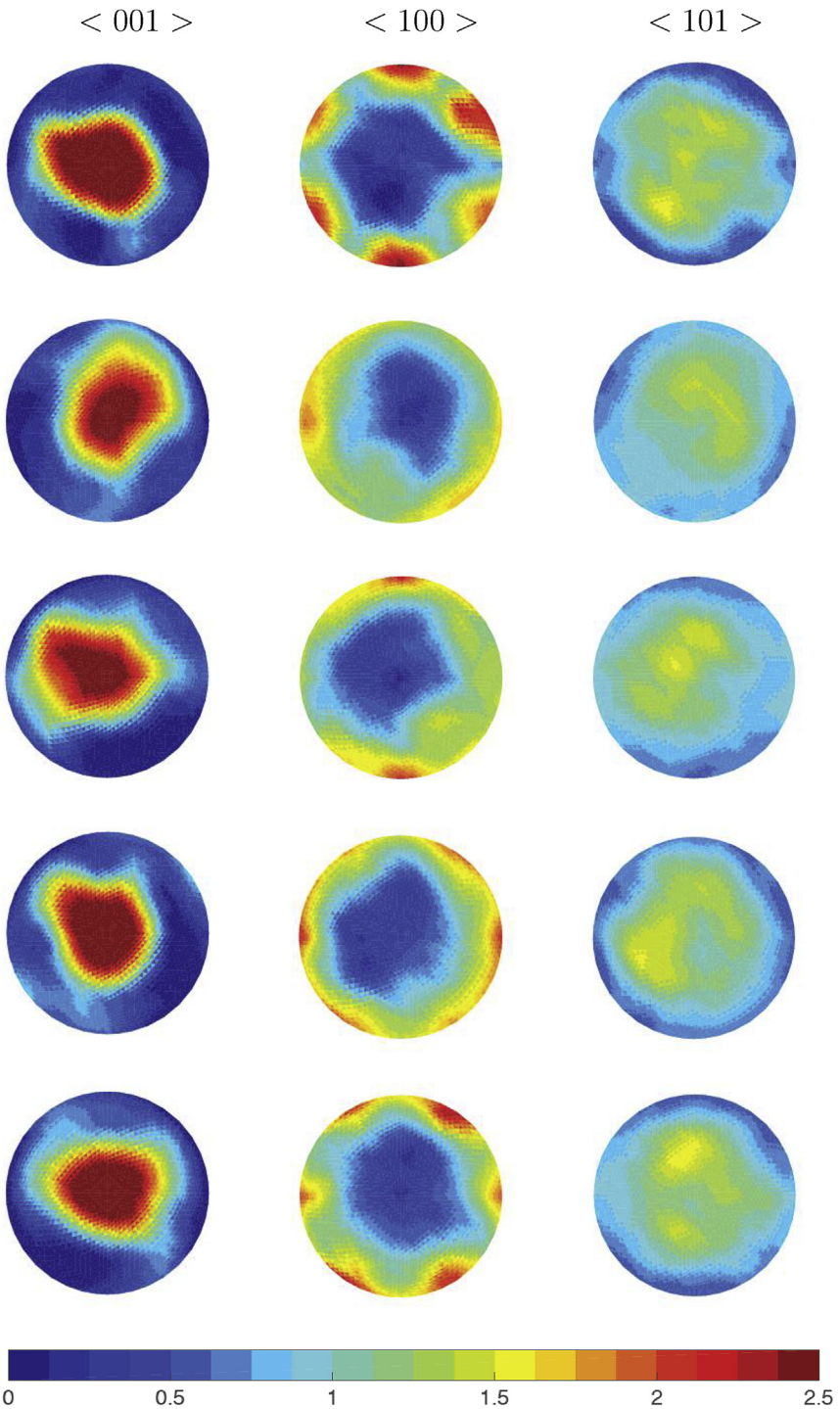

Fig. 3. Representative <001>, <100> and <101> PF samples.

ODFs, including the last ODF (ODF_{50}) are shown in Fig. 6. ODF_{50}, in particular, has a low standard deviation due to the strict normalization constraint. The statistical properties of the ODF distributions (mean values, standard deviations and coefficient of variations of the ODFs) are plotted on the mesh in Fig. 7. We find that some of the ODF values with high mean values also have higher standard deviations. Thus, the coefficient of variation (ratio of standard deviation to mean) of the ODFs is more uniform than the mean or standard devations as indicated by Fig. 7.

The uncertainties in the ODFs and material properties are also quantified using MCS to verify the proposed analytical model. In this approach, we used the aforementioned 100 experimental pole figure sets and directly computed the ODFs from each set, a total of 100 ODFs (using Eq. (2) and the normalization constraint). Then, 100 sets of material properties (S_{11},E_1 etc.) were computed from these ODFs using the homogenization relation (Eq. (3)). Histograms of these ODFs and properties are directly compared to the Gaussian analytical solution. The analytical solution is much faster, the

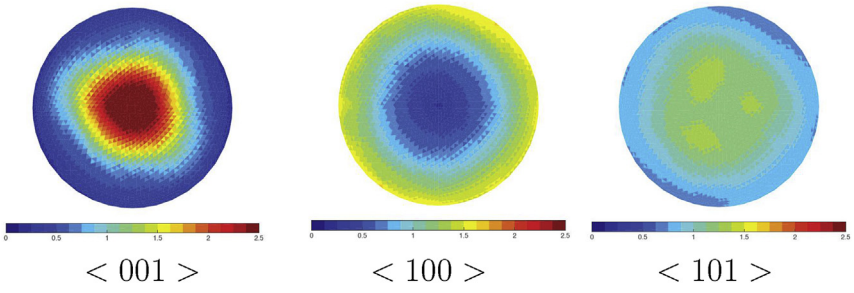

Fig. 4. Mean values of the PFs.

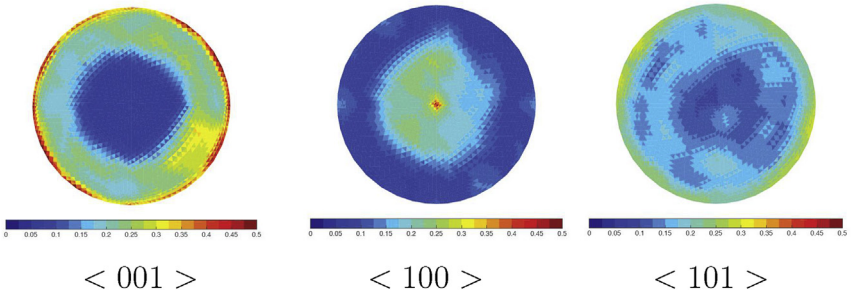

Fig. 5. Coefficient of variations for the PFs.

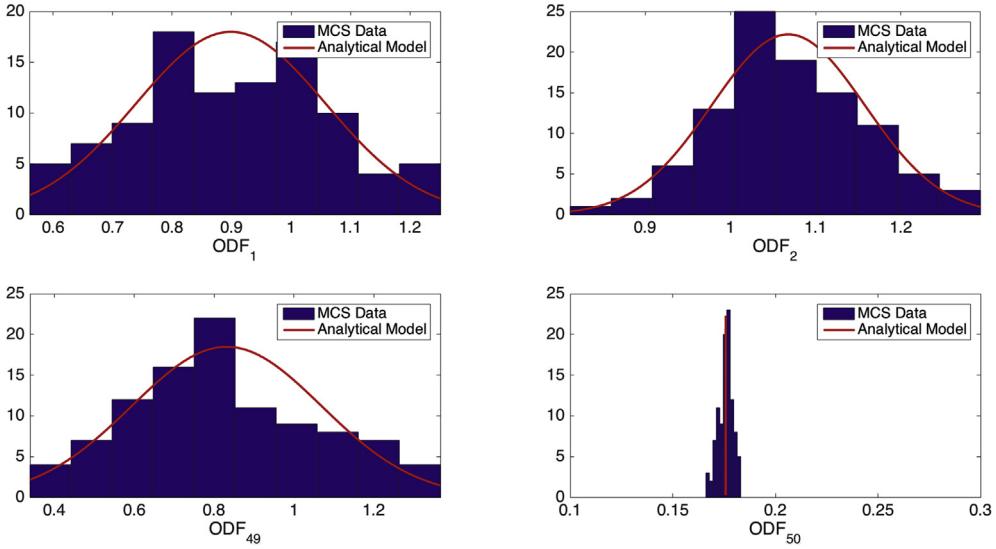

Fig. 6. Probability histograms of the ODFs.

solution times are 7 s for analytical model and 15 min for MCS on the same computational platform. However, MCS provides exact solutions since no Gaussian PDF approximations were made. The MCS results for the probability distributions of ODF_{50}, S_{11}, S_{66}, E_1 and G_{12} are shown together with the analytical model results in Figs. 6, 8 and 9.

Knowing the uncertainty in the ODF, the uncertainties in the homogenized properties were quantified using analysis in Sec. 3.3. The compliance elements, S_{11} and S_{66} are considered using the lower bound approximation. The elastic constants of the single crystals are considered for 750 °C [14], and the values are taken as: $C_{11} = 125.3$ GPa, $C_{12} = 99.4$ GPa, $C_{13} = 68.8$ GPa, $C_{33} = 154.5$ GPa and $C_{55} = 31.6$ GPa. The mean values and standard deviations are computed using Method of Characteristic Functions due to the linear relations of compliance elements with the ODFs. The probability distributions of S_{11} and S_{66} are shown in Fig. 8.

The next step considers the PDFs of the Young's Modulus along sample x– direction, E_1, and shear modulus, G_{12}. Even though the probability distributions of S_{11} and S_{66} are identified as Gaussian, the probability distributions of E_1 and G_{12} are not Gaussian due to their inverse relations ($E_1 = 1/S_{11}$ and $G_{12} = 1/S_{66}$). The PDFs of E_1 and G_{12} are determined using Transformation of Random Variables (Eq. (16)) in Sec. 3.4. To compute these PDFs, the transformation function can be identified as $u(y) = 1/y$ according to relations between E and S_{11}, and G and S_{66}. Then the expected values and the variances are calculated using Eqs. (17) and (18). The probability

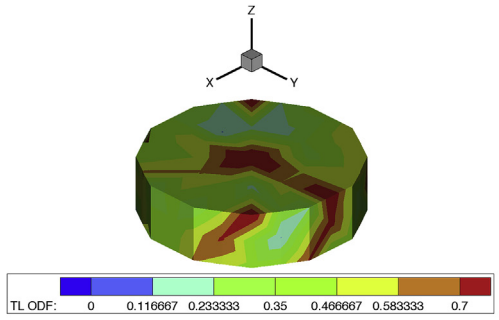

(a) Difference of mean values and standard deviations of the ODFs

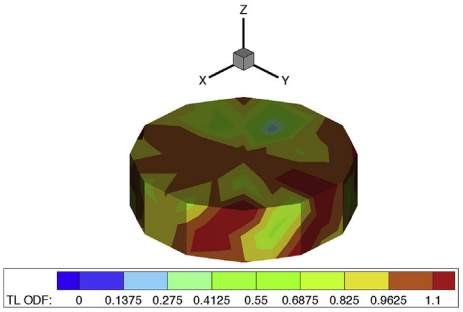

(b) Mean values of the ODFs

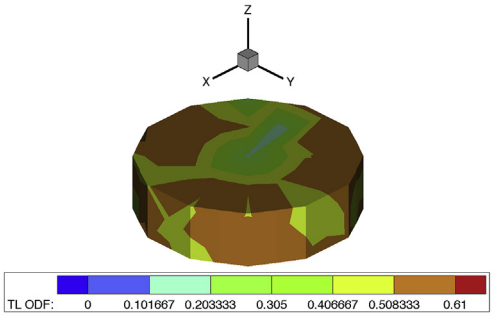

(c) Standard deviations of the ODFs

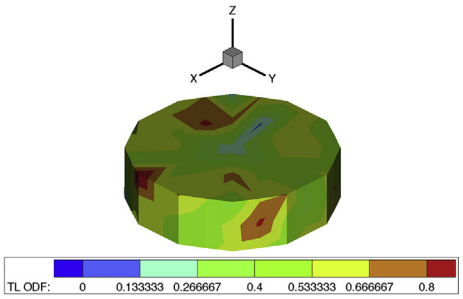

(d) Coefficient of variations of the ODFs

Fig. 7. Statistical features of the ODF probability distributions.

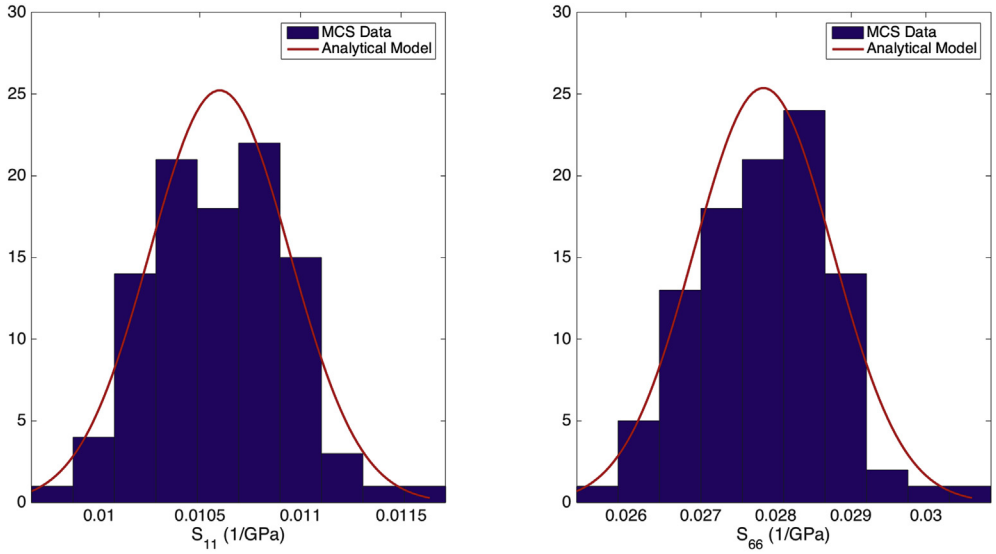

Fig. 8. Probability histograms of S_{11} and S_{66}.

distributions of E_1 and G_{12} are shown in Fig. 9.

The overall analysis is fully analytical when using the Gaussian distribution. However, a drawback of Gaussian distribution is that it allows for negative variables. All the variables considered here, ie. ODFs, pole density functions and the properties are all positive. PDFs with positive variables can instead be considered. Examples of such PDFs include log–normal, exponential, gamma, weibull and rayleigh distributions. Exact analytical treatment of linear system of equations of correlated random variables (eg. Eq. (2)) are not available in literature. Some analytical approximations are available for independent random variables ([15]). However, it is important to note that the pole density functions are highly correlated, as modeled here, and cannot be assumed to be independent. This can be seen from the fact that all pole density functions are derived from the same underlying ODF. The only useful analytical result that the authors could find was the case of correlated sum of

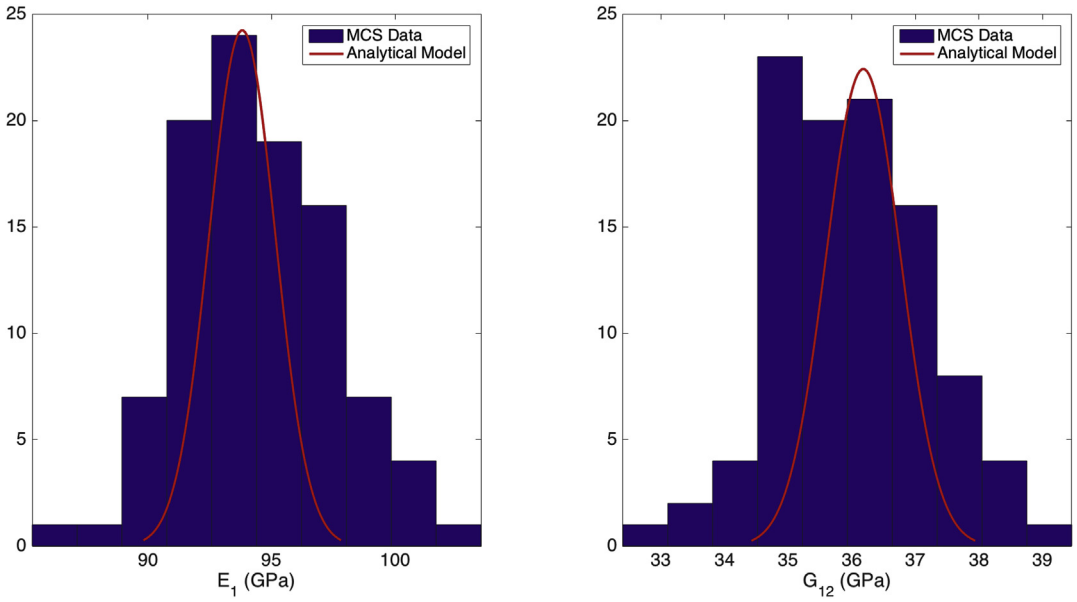

Fig. 9. Probability histograms of E_1 and G_{12}.

Gamma distribution variables with a constant size parameter ([16]). Extension of the approach for a linear system of equations of correlated gamma variables could be pursued in the future. Even so, a gamma distribution has an infinite support. In contrast, the properties have a finite support and are constrained within the extremal values of single crystals [17]. Although a point in the fundamental region can take any value in the positive real axis $(0,\infty)$, numerically the ODF is also modeled to have compact support when the fundamental region is discretized. That is, the values of A_i range from $(0,1/q_i)$. Thus, even with the positive PDFs, we run into issues with exceeding the support space of the modeled variables - similar to the case of a Gaussian distribution. Thus, going beyond Gaussian distributions, one needs to also pursue numerical methods such as MCS and collocation techniques for exact UQ.

From our MCS analysis, we see that the mean values of the probability distributions computed with MCS are in very good agreement with the distributions of the analytical model for the ODF and properties in Figs. 6, 8 and 9. However, the exact variances found from MCS are larger than those from the analytical solution due to the differences between the actual pole figure histograms and the Gaussian approximation as seen in Fig. 2. However, analytical methods are much faster, which is important when stochastic ODFs are employed in multiscale formulations ([18]) of thermomechanical processes.

5. Conclusions

We address analytical techniques for quantification of experimental uncertainties on material properties of microstructures as obtained from volume averaged homogenization relationships. The uncertainties in experimental pole figure data were identified using titanium alloy specimens that were obtained identically through the same process. The uncertainties in the pole figures were quantified using 100 equally sized diffraction samples, and were fitted to a gaussian distribution. The ODF probability distributions were computed using the linear relations and the method of characteristic functions, and they were found to also be consistent with the Gaussian distribution. The mathematical model for the probability distributions of non linear properties was identified using transformation of Random Variables. Using this approach, we calculated the uncertainty bounds in the elastic and shear modulus of the Titanium alloy specimen, that will be useful for engineering models. These derivations are important for development of an ICME toolbox for computing the uncertainty in multiscale homogenization models due to input uncertainties. Analytical representations have the drawback of having an infinite support space compared to the finite support of the discretized ODFs and properties. However, these methods provide a considerable reduction in computational times compared to available numerical techniques. Thus, it is recommended that the Gaussian approach presented here be used as a first step to verify more advanced UQ models. Future effort in this direction includes development of (i) improved methods for building ODFs from crystal aggregate data (using microdiffraction), (ii) methods for modeling linear systems of correlated PDFs with positive support space and (iii) methods for finding PDFs for highly non–linear homogenization relationships. Another interesting UQ problem is the inverse (or materials design) problem of finding the ODF and its uncertainty bounds in order to achieve a set of desired property PDFs.

Acknowledgements

The experimental work presented here was funded by Office of Naval Research (ONR) grant N00014-12-1-0013 and was performed by Anna Trump and Prof John Allison (Materials Science and Engineering) at University of Michigan. The computations have been carried out as part of research supported by the U.S. Department of Energy, Office of Basic Energy Sciences, Division of Materials Sciences and Engineering under Award no. DE-SC0008637 that funds the PRedictive Integrated Structural Materials Science (PRISMS) Center at the University of Michigan.

Appendix A. Formation of property (p) and constraint (q) vectors

ODF is assumed to be discretized into N independent nodes with N_{elem} finite elements and N_{int} integration points per element. The constraint that the ODF is normalized to unity over the fundamental region can then be written as:

$$\int_{\mathcal{R}} \mathcal{A} dv = \sum_{n=1}^{N_{elem}} \sum_{m=1}^{N_{int}} A(\boldsymbol{r}_m) w_m |J_n| \frac{1}{(1+\boldsymbol{r}_m \cdot \boldsymbol{r}_m)^2} = 1 \tag{19}$$

where $A(\boldsymbol{r}_m)$ is the value of the ODF at the m-th integration point with global coordinate $\boldsymbol{r}_m$ of the n-th element, $|J_n|$ is the jacobian determinant of the n-th element and w_m is the integration weight associated with the m-th integration point. This is equivalent to the linear constraint: $\boldsymbol{q}^{intT}\,\boldsymbol{A}^{int} = 1$, where $q_i^{int} = w_i |J_i| \frac{1}{(1+r_i \cdot r_i)^2}$ and $A_i^{int} = A(\boldsymbol{r}_i)$, where $i = 1, \ldots, N_{int} \times N_{elem}$. If the orientation-dependent property for a single crystal $\chi(\boldsymbol{r})$ is known, any polycrystal property can be expressed in a linear form as follows:

$$\langle \chi \rangle = \int_{\mathcal{R}} \chi(\boldsymbol{r}) \mathcal{A}(\boldsymbol{r}) dv = \sum_{n=1}^{nel} \sum_{m=1}^{nint} \chi(\boldsymbol{r}_m) A(\boldsymbol{r}_m) w_m |J_n| \frac{1}{(1+\boldsymbol{r}_m \cdot \boldsymbol{r}_m)^2} \tag{20}$$

This is again equivalent to an equation linear in the ODF: $<\chi = \boldsymbol{p}^{intT}\boldsymbol{A}^{int}$, where $p_i^{int} = \chi(\boldsymbol{r}_i) w_i |J_i| \frac{1}{(1+r_i \cdot r_i)^2}$ and $A_i^{int} = A(\boldsymbol{r}_i)$, $i = 1, \ldots, N_{int} \times N_{elem}$.

Crystallographic symmetry is enforced by considering the set of independent nodal points instead of the integration points. Independent nodal points are the reduced set of nodes obtained by accounting for symmetry conditions at the boundaries of the ODF (see Fig. 1). Let $\boldsymbol{H}$ be the matrix converting the independent nodal values $\boldsymbol{A}^{node}$ to the integration point values $\boldsymbol{A}^{int}$ through the shape functions, then, $\boldsymbol{A}^{int} = \boldsymbol{H}\boldsymbol{A}^{node}$. The independent nodal values $\boldsymbol{A}^{node}$ are sufficient to describe the ODF due to the symmetry of the fundamental region. The ODF constraint can then be written in terms of the modified $\boldsymbol{q}^T = \boldsymbol{q}^{intT}\boldsymbol{H}$ as $\boldsymbol{q}^T\boldsymbol{A}^{node} = 1$. Properties are specified using the modified $\boldsymbol{p}^T \equiv \boldsymbol{p}^{intT}\boldsymbol{H}$ as $<\chi = \boldsymbol{p}^T\boldsymbol{A}^{node}$. In order to account for the normalization constraint $\sum_{i=1}^{k} q_i A_i = 1$, the property vector $\boldsymbol{p}$ is adjusted such that $p_i = p_i - \frac{p_k q_i}{q_k}$ for $i = 1, \ldots, k-1$ and the property rewritten as $<\chi> = \sum_{i=1}^{k-1} p_i A_i + \frac{p_k}{q_k} = \boldsymbol{p}^T\boldsymbol{A} + r$. Vector containing the values of the ODF at first k-1 independent nodal points is hereafter referred to as $\boldsymbol{A}$.

References

[1] J. Allison, D. Backman, L. Christodoulou, Integrated computational materials engineering: a new paradigm for the global materials profession, J. Minerals, Metals Mater. Soc. 58 (11) (2006) 25–27.
[2] A. Creuziger, K. Syed, T. Gnaupel-Herold, Measurement of uncertainty in orientation distribution function calculations, Scr. Mater. 72–73 (2014) 55–58.
[3] L. Juan, G. Liu, H. Wang, A. Ullah, On the sampling of three-dimensional polycrystalline microstructures for distribution determination, J. Microsc. 44 (2) (2011) 214–222.
[4] B. Hiriyur, H. Waisman, G. Deodatis, Uncertainty quantification in homogenization of heterogeneous microstructures modeled by XFEM, Int. J. Numer. Methods Eng. 88 (3) (2011) 257–278.
[5] B. Kouchmeshky, N. Zabaras, The effect of multiple sources of uncertainty on the convex hull of material properties of polycrystals, Comput. Mater. Sci. 47 (2) (2009) 342–352.
[6] P.J. Madrid, D. Sulsky, R.A. Lebensohn, Uncertainty quantification in prediction of the in-plane Young's modulus of thin films with fiber texture, J. Microelectromech. Syst. 23 (2) (2014) 380–390.
[7] S.R. Niezgoda, Y. Yabansu, S.R. Kalidindi, Understanding and visualizing microstructure and microstructure variance as a stochastic process, Acta Mater. 59 (16) (2011) 6387–6400.
[8] N.R. Barton, D.E. Boyce, P.R. Dawson, Pole figure inversion using finite elements over rodrigues space, Textures Microstruct. 35 (2) (2002) 113–144.
[9] T. Chantrasmi, P. Constantine, N. Etemadi, G. Iaccarino, Q. Wang, Uncertainty quantification in simple linear and non-linear problems, Cent. Turbul. Res. Annu. Res. Briefs 1 (2006) 3–16.
[10] H.J. Bunge, Mathematische Methoden der Texturanalyse, Akademie Verlag, Berlin, 1969.
[11] O. Engler, V. Randle, Introduction to Texture Analysis: Macrotexture, Microtexture, and Orientation Mapping, CRC Press (Taylor and Francis), Boca Raton FL, 2000.
[12] A. Gut, An Intermediate Course in Probability, Springer New York, 2009.
[13] S.M. Ross, Introduction to Probability Models, tenth ed., *Elsevier*, 2010.
[14] G. Simmons, H. Wang, Single Crystal Elastic Constants and Calculated Aggregate Properties, The M.I.T Press, 1971.
[15] S. Nadarajah, A review of results on sums of random variables, Acta Appl. Math. 103 (2008) 131–140.
[16] M.S. Alouini, A. Abdi, M. Kaveh, Sum of gamma variates and performance of wireless sommunications systems over Nakagami fading channels, IEEE Trans. Veh. Technol. 50 (2001) 1471–1480.
[17] V. Sundararaghavan, N. Zabaras, Linear analysis of textureproperty relationships using process-based representations of Rodrigues space, Acta Mater. 55 (2007) 1573–1587.
[18] V. Sundararaghavan, N. Zabaras, A multi-length scale continuum sensitivity analysis for the control of texture-dependent properties in deformation processing, Int. J. Plasticity 24 (2008) 1581–1605.